Orbital engineering in YVO₃-LaAlO₃ superlattices

P. Radhakrishnan [1] B. Geisler [2] K. Fürsich [1] D. Putzky,[1] Y. Wang,[1] S. E. Ilse [3] G. Christiani,[1] G. Logvenov,[1]
P. Wochner,[1] P. A. van Aken [1] E. Goering,[3] R. Pentcheva [2] and E. Benckiser [1,*]

[1]*Max Planck Institute for Solid State Research, Heisenbergstrasse 1, 70569 Stuttgart, Germany*
[2]*Department of Physics and Center for Nanointegration (CENIDE), Universität Duisburg-Essen, Lotharstrasse 1, 47057 Duisburg, Germany*
[3]*Max Planck Institute for Intelligent Systems, Heisenbergstrasse 3, 70569 Stuttgart, Germany*

Oxide heterostructures provide unique opportunities to modify the properties of quantum materials through a targeted manipulation of spin, charge, and orbital states. Here, we use resonant x-ray reflectometry to probe the electronic structure of thin slabs of YVO₃ embedded in a superlattice with LaAlO₃. We extend the previously established methods of reflectometry analysis to a general form applicable to t_{2g} electron systems and extract quantitative depth-dependent x-ray linear dichroism profiles. Our data reveal an artificial, layered orbital polarization, where the average occupation of xz and yz orbitals in the interface planes next to LaAlO₃ is inverted compared to the central part of the YVO₃ slab. This phase is stable down to 30 K and the bulklike orbital ordering transitions are absent. We identify the key mechanism for the electronic reconstruction to be a combination of epitaxial strain and spatial confinement by the LaAlO₃ layers, in good agreement with predictions from *ab initio* theory.

DOI: 10.1103/PhysRevB.104.L121102

Heterostructures offer new opportunities to manipulate quantum materials and create novel and technologically relevant phases, such as superconductivity and magnetism. One possibility for the targeted manipulation of quantum states is the epitaxial stabilization of certain orbital occupations, which is pursued in the so-called *orbital engineering*. Such local modifications of orbital occupations and orbital overlap are decisive for the strength and sign of magnetic superexchange interactions [1,2], and therefore stabilize new artificial spin orders. They are of great fundamental interest [3] and could find important practical applications in future (antiferromagnetic)-spintronic devices [4,5] and all-oxide solar cells [6]. The success of these efforts will crucially depend on a thorough understanding of the underlying mechanisms and their hierarchy. This is the central motivation of our Letter, in which we verify a detailed picture of the reconstructions in a prototypical correlated-electron system.

In rare-earth vanadates (RVO₃), the interactions between spin, orbital, and lattice degrees of freedom lead to a complex phase diagram, consisting of various spin and orbital orders [7]. In particular, bulk YVO₃ (YVO) undergoes a series of temperature-dependent phase transitions; a *G*-type orbital ordering transition at ∼200 K, *C*-type spin ordering at ∼116 K, and finally a *C*-type orbital/*G*-type spin ordering at ∼77 K

[8,9]. RVO₃ crystallize in a perovskite-type orthorhombic structure (space group *Pbnm*) where the V³⁺ ions have a t_{2g}^2 electronic configuration at each vanadium site [Fig. 1(a)]. The first electron always occupies the xy orbital, and the second one occupies either the yz or xz orbital, depending upon the crystallographic direction and the spin-orbital phase. The relatively low onset temperature of orbital order and the associated small energy scales of orbital excitations have led to some proposals about a collective nature of orbital excitations [10,11], which were later supported by different experimental studies [12–17]. While the rich physics of vanadates has been widely studied in bulk form, thin films and multilayers have been far less investigated [18]. Most reported studies have focused on a possible charge transfer at polar interfaces of LaVO₃-Sr(V, Ti)O₃ [19,20], and more recently on the influence of different oxide substrates on the magnetic properties of epitaxial PrVO₃ films [21]. Over the past few years, heteroepitaxial modifications of orbital occupations have been tested in several studies for systems with partially filled e_g orbitals [22–28]. In this Letter, we use resonant reflectometry to test the effects of multiple heterointerfaces on the orbital physics in vanadates, a t_{2g} electron system, where the orbital-lattice coupling is expected to be smaller. This technique was used to derive qualitative information about the electronic reconstruction at the interface of several superlattices [29–31]. A quantitative analysis was performed for the e_g electron system of nickelate superlattices to extract its orbital polarization profiles [32,33]. Here, we extend that analysis to a more general form applicable to t_{2g} systems and extract the quantitative depth-resolved electronic structure of YVO.

To this end, we have investigated a set of superlattice structures, composed of YVO and the wide band-gap insulator
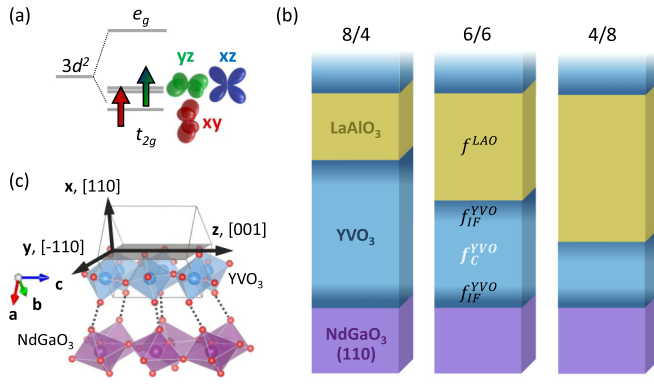
FIG. 1. (a) Orbital occupation of V^{3+} ion in RVO_3. Since the configuration mixing of the lowest triplet states ($^3T_1$) is small in the d^2 system, the use of the single electron basis (t_{2g}^2) is justified and we will refer to it throughout this Letter. (b) Sketch of the 8/4, 6/6, and 4/8 superlattice structures. For all three, the YVO-LAO bilayers are repeated six times. (c) Orientation of the orthorhombic YVO unit cell, with lattice parameters a, b, and c

FIG. 2. Characterization of the 8/4 sample. (a) HAADF image showing YVO and LAO layers. (b) STEM-EELS displaying elemental compositions of V, La, Y, and Al in the SL. (c) XAS of the V-$L_{2,3}$ and O-K edge. (d) STEM-EELS V-$L_{2,3}$ edge line spectra at different positions across the YVO slab (see inset).

LaAlO₃ (LAO), sketched in Fig. 1(b). We designed superlattices (SLs) with stacking sequences of YVO/LAO: (8/4) × 6, (6/6) × 6, and (4/8) × 6 pseudocubic unit cells. These were chosen specifically, since different superlattice reflections with a given momentum transfer (Q) have different sensitivities to interfacial reconstructions. We assign the scattering factors, f_C^{YVO} and f_{IF}^{YVO} for the central (C) and interfacial (IF) layers within YVO, and f^{LAO} for LAO [Fig. 1(b)]. For the 6/6 SL, we expect the intensity of the (002) superlattice reflection to be proportional to $f_{IF}^{YVO} - f_C^{YVO}$, i.e., sensitive to interfacial reconstructions. For the 4/8 and 8/4 SLs, the same is expected for the (003) superlattice reflection. Using a combination of our heterostructure design, polarization-dependent resonant x-ray reflectivity [32,34], and *ab initio* theory allowed us to determine its layer-resolved electronic structure and provided insight into the origin of the observed modifications.

All three SLs were grown by pulsed-laser deposition in ultrahigh vacuum, using a KrF laser ($\lambda = 248$ nm) on NdGaO₃ (110) substrates. A fluence of 2 J/cm² with a repetition rate of 5 Hz was used to ablate a polycrystalline target of YVO₄. The oxygen partial pressure and substrate temperature were optimized at about 10^{-7} mbar and 700 °C, respectively. With reference to the geometry shown in Fig. 1(c), YVO is under tensile strains of 0.31% and 1.66% along the [−110] and [001] directions, respectively. LAO is also under tensile strains of 1.6% and 1.3% along the [−110] and [001] directions, respectively.

We characterized the samples using x-ray diffraction (XRD), x-ray absorption spectroscopy (XAS), and scanning transmission electron microscopy (STEM) (see details in the Supplemental Material [35]). Polarized XAS and resonant x-ray reflectivity measurements were carried out at the UE56-2 PGM-2 beamline in BESSY, Berlin, using the ultrahigh vacuum reflectometer described in Ref. [36]. We simulated the reflectivity using the software tool REMAGX [34] and performed full-multiplet ligand-field cluster calculations using QUANTY [37–39]. STEM measurements were made using a JEOL JEM-ARM 200F scanning transmission electron microscope. We performed first-principles calculations in the
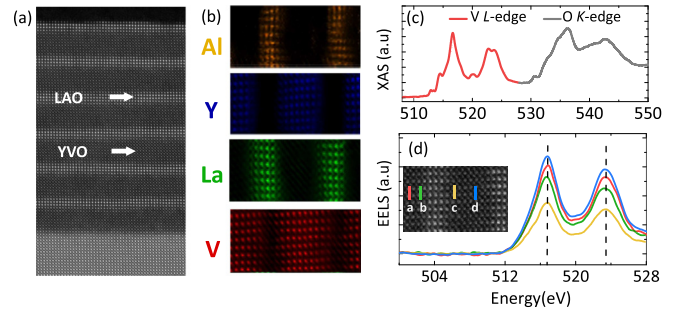
framework of spin-polarized density functional theory [40] (DFT) as implemented in the QUANTUM ESPRESSO code [41]. The generalized gradient approximation was used for the exchange-correlation functional as parametrized by Perdew, Burke, and Ernzerhof [42]. Static correlation effects were considered within the DFT + U formalism [43] ($U_V = 3$ eV). To account for octahedral rotations, orbital order, and magnetic order simultaneously, we model the SLs by using a large $p(2 \times 2)$ 4/4 SL supercell that adopts the experimentally determined geometry, with four pseudocubic unit cells per layer. In addition, we explicitly treat interfacial Y-La intermixing. All atomic positions were accurately optimized.

STEM-HAADF (high-angle annular dark-field) and EELS (electron energy-loss spectroscopy) elemental mapping revealed that chemical intermixing and interfacial roughness are confined to about two atomic layers [Figs. 2(a) and 2(b)]. We probed the stoichiometry of the sample using a combination of XAS and atomic-layer resolved EELS, both measured across the V-$L_{2,3}$ edge. XAS revealed the oxidation state of vanadium to be 3+ [Fig. 2(c)] and EELS yielded constant positions of the peaks when measured through the YVO slab [Fig. 2(d)]. This suggests that the V^{3+} state is preserved throughout the slab [44]. Electronic transport measurements showed a highly insulating behavior, similar to that observed in bulk YVO single crystals [45].

We determined the depth-resolved, layer-averaged electronic structure by analyzing the resonant reflectometry data (Fig. 3). In the first step, a structural model was obtained by simultaneously fitting the Q-dependent reflectivity at different energies [see Fig. 3(a) and the Supplemental Material [35]]. For this purpose, the XAS spectra measured with polarization along the x, y, and z directions [Fig. 3(d)] were used to build resonant optical constants (scattering factors) of YVO and LAO and their corresponding dielectric tensors (see also Ref. [32]). The structural model was then kept fixed for the subsequent analysis. The next step consisted of simulating the energy-dependent reflectivity at constant Q and comparing the results to the experimental curves [Fig. 3(b)]. Since YVO is under asymmetric epitaxial strain (i.e., different strain along [−110] and [001] directions) and is a t_{2g} system, our analysis method required alterations compared to Ref. [32], where an e_g system on a square lattice substrate was investigated (see Supplemental Material [35]). We found a unique
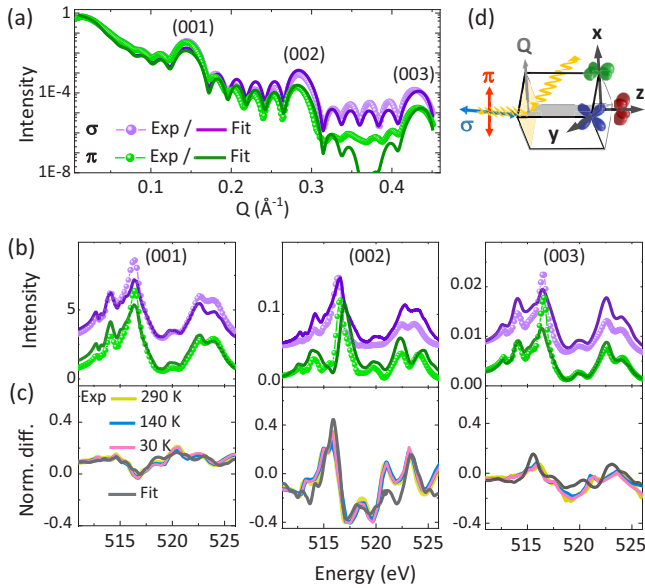
FIG. 3. Resonant reflectivity of the (4/8) SL at room temperature (a) at fixed energy of 516.7 eV as a function of Q, and (b) as a function of energy across the V-$L_{2,3}$ edge at the fixed momentum transfer of superlattice reflections: $Q_{(001)} = 0.147$ Å^{-1}, $Q_{(002)} = 0.285$ Å^{-1}, and $Q_{(003)} = 0.430$ Å^{-1}. Experimental and simulated spectra shown for σ and π polarizations. (c) The constant-Q dichroism defined as $(I_\sigma - I_\pi)/(I_\sigma + I_\pi)$ shown for simulated and measured spectra for different temperatures of 30, 140, and 290 K. (d) Scattering geometry with respect to the YVO unit cell and frame of reference of the orbitals.

FIG. 4. (a) Experimental (circles) and fitted (lines) linear dichroism profiles between two pairs of polarizations for the central (C) layers of all three stackings (top) and the interfacial (IF) layers of 8/4, 6/6, and 4/8 SLs. (b) Schematic showing the orbital polarization for bulk, C, and IF layers of the SLs with normalized orbital polarizations $P_1 = (n_{xz} - n_{yz})/(n_{xz} + n_{yz})$ and $P_2 = [n_{xy} - (n_{xz} + n_{yz})/2]/[n_{xy} + (n_{xz} + n_{yz})/2]$ in %, both within an error of $\pm 2\%$. (c) Layer-resolved, site-averaged, and orbital-projected density of states of a representative 4/4 YVO-LAO SL obtained from DFT + U. The green and blue curves correspond to V yz and xz orbitals, respectively, and reveal a distinct lifting of the orbital degeneracy in C vs IF layers.

depth-dependent x-ray linear dichroism (XLD) profile for each sample, when all superlattice reflections $(00L)$, $L = 1$, 2, 3 were fit simultaneously [Fig. 3(c)]. For all three stacking sequences, the interface layer in YVO is about one unit cell thick, as sketched by a darker shade in Fig. 1(b). As will be discussed below, these interfacial layers show an inverted orbital occupation compared to the central part of the YVO slab [lighter shade in Fig. 1(b)]. The temperature independence of the dichroism of constant-Q reflectivity [Fig. 3(c)] implies that this orbital occupation pattern is stable from 290 K down to 30 K. Bulk YVO shows significant changes in the size and shape of the XLD through the orbital ordering transitions, where it nearly doubles in size upon lowering the temperature below 200 K [46]. The negligible differences through temperature in our data indicate the absence of bulklike phase changes in the SLs. This suggests that heterostructuring has created a significant alteration of the electronic properties with respect to bulk YVO.

The XLD profiles, extracted from the imaginary parts of the modeled scattering factors f_{IF}^{YVO} and f_C^{YVO}, are shown in Fig. 4(a). To determine the orbital occupations in a quantitative manner, we performed full-multiplet ligand-field cluster calculations and compared them with the XLD profiles. The octahedra of bulk YVO have D_{2h} symmetry, i.e., three different V-O bond lengths, but the average bond lengths along the x and y directions are equal at room temperature. Thus, the layer-averaged orbital occupations of yz and xz orbitals are also equal [46,47]. The final results of our simulations are an average of spectra from two inequivalent in-plane V sites,

each with D_{2h} symmetry and different ligand fields, projected onto the polarization vectors. In contrast to bulk YVO, both the C and IF layers show a sizable linear dichroism between the x and y directions. Within our error bar, the C layers of all three superlattices show identical spectra, whereas the IF layers show differences between the z and x polarization. Comparing the C and IF layers' spectra, the most striking result is the reversal of the sign of x-y linear dichroism.

The orbital occupations determined from the cluster calculations were normalized to have a total occupation of two electrons in the t_{2g} manifold. To quantify orbital polarizations, we use parameters P_1, defined between the difference in occupation of xz and yz orbitals, and P_2, defined similarly between those of xy and the average of xz, yz orbitals (see the caption of Fig. 4 for the exact definition of $P_{1,2}$). As indicated by the linear dichroism, the C layers of all three superlattices have similar P_1 and P_2 [Fig. 4(b)]. The C and IF layers show a reversal of orbital polarization, i.e., have opposite sign of P_1, corresponding to a higher occupation of xz in the C layers and a higher yz occupation in the IF layers. Additionally, the IF layers exhibit an increase in P_2, when going from 8/4, to 6/6, to 4/8 stacking.

Qualitatively, we explain these trends by a combined effect of structural modifications imposed by the substrate and spatial confinement by the LAO layers at the interface. The preservation of the orthorhombic crystal symmetry results in the first electron occupying the xy orbital at each vanadium site, as in bulk YVO. However, the heteroepitaxial modifications influence the occupation of the second orbital. Since metal d orbitals are antibonding in nature, an increase in

the lattice parameter which is associated with longer bonds, lowers the energy of the orbital with lobes extended in that direction. Thus, the preferential xz orbital occupation obtained for the C layers is expected for an elongated out-of-plane lattice parameter. Our XRD measurements indicated that the YVO slabs in the SL indeed exhibit a larger out-of-plane lattice parameter, despite being under tensile strain; this was also confirmed by DFT (see Supplemental Material [35]).

The reversal of the sign of P_1 in the interface layers is attributed to the effect of spatial confinement. Since LAO is a wide-band gap insulator with a closed-shell electronic configuration of Al^{3+}, hopping along the V-O-Al bonds across the interface is strongly diminished. This leads to spatial confinement of the electrons at the interface and a preferred in-plane orbital occupation compared to bulk and C layers. In our geometry, this produces an inverted occupation of the xz and yz orbitals. As the effects of both epitaxial strain and spatial confinement differentiate between the in-plane and out-of-plane directions, the orientation of the unit cell with its c axis in plane is crucial, since it places the yz orbital in the plane of the substrate surface. This enables the possibility to lift the degeneracy as opposed to the orientation with the c axis out of plane (i.e., xy orbital in plane). Additionally, xz and yz are also the ordering orbitals in the low-temperature phases of the bulk phase, and thus lifting the degeneracy between these two orbitals is expected to have a profound impact on the orbital ordering and the low-temperature physics of YVO. The lack of temperature dependence of the reflectometry data strongly suggests that the electronic structure is preserved down to at least 30 K. This has possibly important consequences for the associated magnetic order which is determined by the Goodenough-Kanamori rules [1,2] for superexchange interactions. Our results demonstrate that the choice of a specific orientation of the substrate can be used to predictably engineer orbital polarization through epitaxial strain and spatial confinement.

The monotonic increase of P_2 in the IF layers for different stacking sequences possibly arises from a combination of structural distortions induced by LAO and the confinement effect. To maintain octahedral connectivity with LAO, YVO needs to locally distort at the interface, since the respective bulk structures have different lattice parameters and crystal symmetry ($R\bar{3}c$ for LAO and *Pbnm* for YVO). Going from (8/4) to (4/8) SLs, the size of the distortion increases with the ratio of LAO thickness to that of YVO, but simultaneously, the size of the confinement effect is also enhanced. From our current set of data, it is not possible to fully disentangle these two effects, but they explain why P_2 of the sample with the smallest LAO slab thickness (8/4 sample) is similar to that of bulk and C layers.

To verify our experimental observations, we performed first-principles simulations of a representative 4/4 YVO-LAO SL [Fig. 4(c)]. We find an in-plane G-type spin and C-type orbital ordered ground state for C and IF YVO layers. While the overall electronic structure of the C layers resembles bulk YVO with V-t_{2g} states located deep in the band gap of the insulating LAO (the valence band maximum of LAO is located at about -2.5 eV), we clearly observe that the xz, yz orbital degeneracy is lifted, with a lower energy of the occupied xz bands. An inverted occupation scheme is seen in the IF layers, where the occupied yz states are lower in energy. The energy splitting $\Delta\epsilon = \epsilon_{xz} - \epsilon_{yz}$ amounts to $\Delta\epsilon = -110$ meV (C) and $+50$ meV (IF), if the peak energies are considered [as marked in Fig. 4(c)] and $\Delta\epsilon = -8$ meV (C) and $+21$ meV (IF), if the band center energies are used. The latter are defined as $\epsilon_i = \int_{-\infty}^{E_F} dE\, E\, g_i(E) / \int_{-\infty}^{E_F} dE\, g_i(E)$, $i = xz, yz$, with the orbital-resolved and site-averaged density of states $g_i(E)$ and the Fermi energy E_F. From a statistical perspective, this distinct energy-level sequence in C vs IF layers implies that the xz orbital is more often occupied at the V sites in the C layers, whereas the yz orbital is preferentially occupied at the V sites in the IF layers, hence giving rise to a finite orbital polarization.

In summary, we have used resonant x-ray reflectometry in combination with configuration-interaction cluster calculations and *ab initio* theory to understand the impact of heterostructuring in a correlated t_{2g}^2 electron system. We obtained quantitative depth-resolved electronic structure profiles with an unprecedented level of detail and find a clear alteration of orbital polarization in YVO-LAO superlattices compared to bulk YVO. Heterostructuring creates an overall preferential orbital occupation, with the reversal of orbital polarization of xz and yz orbitals, between the C and IF layers within the YVO slab. Furthermore, it also suppresses the orbital ordering phase transitions present in the bulk. These changes in the electronic structure are attributed to the specific orientation of the unit cell, epitaxial strain, and spatial confinement at the interface, based on detailed XRD, TEM measurements, and *ab initio* calculations. Such an understanding and differentiation of the effects of structural and electronic modifications via heteroepitaxy as well as the reliable predictability of first-principles simulations, paves the way for a rational design of quantum materials with different functionalities.

[1] J. Kanamori, J. Phys. Chem. Solids **10**, 87 (1959).

[2] J. B. Goodenough, Phys. Rev. **100**, 564 (1955).

[3] D. Gotfryd, E. M. Pärschke, J. Chaloupka, A. M. Oleś, and K. Wohlfeld, Phys. Rev. Research **2**, 013353 (2020).

[4] V. Baltz, A. Manchon, M. Tsoi, T. Moriyama, T. Ono, and Y. Tserkovnyak, Rev. Mod. Phys. **90**, 015005 (2018).

[5] M. Bibes and A. Barthelemy, IEEE Trans. Electron Devices **54**, 1003 (2007).

[6] E. Assmann, P. Blaha, R. Laskowski, K. Held, S. Okamoto, and G. Sangiovanni, Phys. Rev. Lett. **110**, 078701 (2013).

[7] S. Miyasaka, Y. Okimoto, M. Iwama, and Y. Tokura, Phys. Rev. B **68**, 100406(R) (2003).

[8] G. R. Blake, T. T. M. Palstra, Y. Ren, A. A. Nugroho, and A. A. Menovsky, Phys. Rev. Lett. **87**, 245501 (2001).

[9] Y. Ren, T. Palstra, D. Khomskii, E. Pellegrin, A. A. Nugroho, A. A. Menovsky, and G. A. Sawatzky, Nature (London) **396**, 441 (1998).

[10] G. Khaliullin, P. Horsch, and A. M. Oleś, Phys. Rev. Lett. **86**, 3879 (2001).

[11] S. Ishihara, Phys. Rev. B **69**, 075118 (2004).

[12] D. J. Lovinger, M. Brahlek, P. Kissin, D. M. Kennes, A. J. Millis, R. Engel-Herbert, and R. D. Averitt, Phys. Rev. B **102**, 115143 (2020).

[13] S. Miyasaka, J. Fujioka, M. Iwama, Y. Okimoto, and Y. Tokura, Phys. Rev. B **73**, 224436 (2006).

[14] S. Sugai and K. Hirota, Phys. Rev. B **73**, 020409(R) (2006).

[15] C. Ulrich, G. Khaliullin, J. Sirker, M. Reehuis, M. Ohl, S. Miyasaka, Y. Tokura, and B. Keimer, Phys. Rev. Lett. **91**, 257202 (2003).

[16] E. Benckiser, R. Rückamp, T. Möller, T. Taetz, A. Möller, A. A. Nugroho, T. T. M. Palstra, G. S. Uhrig, and M. Grüninger, New J. Phys. **10**, 053027 (2008).

[17] E. Benckiser, L. Fels, G. Ghiringhelli, M. Moretti Sala, T. Schmitt, J. Schlappa, V. N. Strocov, N. Mufti, G. R. Blake, A. A. Nugroho, T. T. M. Palstra, M. W. Haverkort, K. Wohlfeld, and M. Grüninger, Phys. Rev. B **88**, 205115 (2013).

[18] M. Brahlek, L. Zhang, J. Lapano, H.-T. Zhang, R. Engel-Herbert, N. Shukla, S. Datta, H. Paik, and D. G. Schlom, MRS Commun. **7**, 27 (2017).

[19] A. David, R. Frésard, P. Boullay, W. Prellier, U. Lüders, and P.-E. Janolin, Appl. Phys. Lett. **98**, 212106 (2011).

[20] H. Rotella, O. Copie, A. Pautrat, P. Boullay, A. David, D. Pelloquin, C. Labbé, C. Frilay, and W. Prellier, J. Phys.: Condens. Matter **27**, 095603 (2015).

[21] D. Kumar, A. David, A. Fouchet, A. Pautrat, J. Varignon, C. U. Jung, U. Lüders, B. Domengès, O. Copie, P. Ghosez, and W. Prellier, Phys. Rev. B **99**, 224405 (2019).

[22] G. Fabbris, D. Meyers, J. Okamoto, J. Pelliciari, A. S. Disa, Y. Huang, Z.-Y. Chen, W. B. Wu, C. T. Chen, S. Ismail-Beigi, C. H. Ahn, F. J. Walker, D. J. Huang, T. Schmitt, and M. P. M. Dean, Phys. Rev. Lett. **117**, 147401 (2016).

[23] M. Wu, E. Benckiser, M. W. Haverkort, A. Frano, Y. Lu, U. Nwankwo, S. Brück, P. Audehm, E. Goering, S. Macke, V. Hinkov, P. Wochner, G. Christiani, S. Heinze, G. Logvenov, H.-U. Habermeier, and B. Keimer, Phys. Rev. B **88**, 125124 (2013).

[24] F. Wrobel, B. Geisler, Y. Wang, G. Christiani, G. Logvenov, M. Bluschke, E. Schierle, P. A. van Aken, B. Keimer, R. Pentcheva, and E. Benckiser, Phys. Rev. Materials **2**, 035001 (2018).

[25] P. Chen, Z. Huang, M. Li, X. Yu, X. Wu, C. Li, N. Bao, S. Zeng, P. Yang, L. Qu, J. Chen, J. Ding, S. J. Pennycook, W. Wu, T. V. Venkatesan, A. Ariando, and G. M. Chow, Adv. Funct. Mater. **30**, 1909536 (2020).

[26] B. Geisler and R. Pentcheva, Phys. Rev. Applied **11**, 044047 (2019).

[27] D. Doennig, W. E. Pickett, and R. Pentcheva, Phys. Rev. B **89**, 121110(R) (2014).

[28] B. Geisler and R. Pentcheva, Phys. Rev. B **102**, 020502(R) (2020).

[29] Ş. Smadici, P. Abbamonte, A. Bhattacharya, X. Zhai, B. Jiang, A. Rusydi, J. N. Eckstein, S. D. Bader, and J.-M. Zuo, Phys. Rev. Lett. **99**, 196404 (2007).

[30] J. Park, B.-G. Cho, K. D. Kim, J. Koo, H. Jang, K.-T. Ko, J.-H. Park, K.-B. Lee, J.-Y. Kim, D. R. Lee, C. A. Burns, S. S. A. Seo, and H. N. Lee, Phys. Rev. Lett. **110**, 017401 (2013).

[31] H. Wadati, D. G. Hawthorn, J. Geck, T. Higuchi, Y. Hikita, H. Y. Hwang, L. F. Kourkoutis, D. A. Muller, S.-W. Huang, D. J. Huang, H.-J. Lin, C. Schüßler-Langeheine, H.-H. Wu, E. Schierle, E. Weschke, N. J. C. Ingle, and G. A. Sawatzky, J. Appl. Phys. **106**, 083705 (2009).

[32] E. Benckiser, M. W. Haverkort, S. Brück, E. Goering, S. Macke, A. Frano, X. Yang, O. K. Andersen, G. Cristiani, H. U. Habermeier, A. V. Boris, I. Zegkinoglou, P. Wochner, H. J. Kim, V. Hinkov, and B. Keimer, Nat. Mater. **10**, 189 (2011).

[33] M. Wu, E. Benckiser, P. Audehm, E. Goering, P. Wochner, G. Christiani, G. Logvenov, H.-U. Habermeier, and B. Keimer, Phys. Rev. B **91**, 195130 (2015).

[34] S. Macke, A. Radi, J. E. Hamann-Borrero, A. Verna, M. Bluschke, S. Brück, E. Goering, R. Sutarto, F. He, G. Cristiani, M. Wu, E. Benckiser, H.-U. Habermeier, G. Logvenov, N. Gauquelin, G. A. Botton, A. P. Kajdos, S. Stemmer, G. A. Sawatzky, M. W. Haverkort, Adv. Mater. **26**, 6554 (2014).

[35] See Supplemental Material at http://link.aps.org/supplemental/10.1103/PhysRevB.104.L121102 for further details of XRD used to verify the structure of YVO$_3$ inside the SL, the description of scattering factor models, uniqueness of XLD profiles, and sensitivity of x-ray reflectometry, which includes Refs. [50–54].

[36] S. Brück, S. Bauknecht, B. Ludescher, E. Goering, and G. Schütz, Rev. Sci. Instrum. **79**, 083109 (2008).

[37] M. W. Haverkort, M. Zwierzycki, and O. K. Andersen, Phys. Rev. B **85**, 165113 (2012).

[38] Y. Lu, M. Höppner, O. Gunnarsson, and M. W. Haverkort, Phys. Rev. B **90**, 085102 (2014).

[39] M. W. Haverkort, G. Sangiovanni, P. Hansmann, A. Toschi, Y. Lu, and S. Macke, Europhys. Lett. **108**, 57004 (2014).

[40] W. Kohn and L. J. Sham, Phys. Rev. **140**, A1133 (1965).

[41] P. Giannozzi, S. Baroni, N. Bonini, M. Calandra, R. Car, C. Cavazzoni, D. Ceresoli, G. L. Chiarotti, M. Cococcioni, I. Dabo, A. Dal Corso, S. de Gironcoli, S. Fabris, G. Fratesi, R. Gebauer, U. Gerstmann, C. Gougoussis, A. Kokalj, M. Lazzeri, L. Martin-Samos *et al.*, J. Phys.: Condens. Matter **21**, 395502 (2009).

[42] J. P. Perdew, K. Burke, and M. Ernzerhof, Phys. Rev. Lett. **77**, 3865 (1996).

[43] M. Cococcioni and S. de Gironcoli, Phys. Rev. B **71**, 035105 (2005).

[44] L. F. Kourkoutis, Y. Hotta, T. Susaki, H. Y. Hwang, and D. A. Muller, Phys. Rev. Lett. **97**, 256803 (2006).

[45] M. Kasuya, Y. Tokura, T. Arima, H. Eisaki, and S. Uchida, Phys. Rev. B **47**, 6197 (1993).

[46] N. Hollmann, Ph.D. thesis, University of Cologne, 2010.

[47] Since $I_x - I_y$ and $I_z - I_x$ are proportional to $\bar{n}_{yz} - \bar{n}_{xz}$ and $\bar{n}_{xy} - \bar{n}_{yz}$, respectively, where $\bar{n}$ refers to the holes residing in a given orbital [48,49].

[48] B. T. Thole, P. Carra, F. Sette, and G. van der Laan, Phys. Rev. Lett. **68**, 1943 (1992).

[49] P. Carra, H. König, B. Thole, and M. Altarelli, Phys. B: Condens. Matter **192**, 182 (1993).

[50] A. Vailionis, H. Boschker, W. Siemons, E. P. Houwman, D. H. A. Blank, G. Rijnders, and G. Koster, Phys. Rev. B **83**, 064101 (2011).

[51] C. T. Chantler, J. Phys. Chem. Ref. Data **29**, 597 (2000).

[52] R. Nakajima, J. Stöhr, and Y. U. Idzerda, Phys. Rev. B **59**, 6421 (1999).

[53] A. Ruosi, C. Raisch, A. Verna, R. Werner, B. A. Davidson, J. Fujii, R. Kleiner, and D. Koelle, Phys. Rev. B **90**, 125120 (2014).

[54] J. Hwang, J. Son, J. Y. Zhang, A. Janotti, C. G. Van de Walle, and S. Stemmer, Phys. Rev. B **87**, 060101(R) (2013).